

Non-linear Control of Grid-Side Inverters [★]

Alexander Schöley* Magdalena Gierschner**
Torsten Jeinsch*

* *University of Rostock, Institute of Automation, Rostock, Germany*
(e-mail: alexander.schoeley@uni-rostock.de)

** *University of Rostock, Institute for Electrical Power Engineering,*
Rostock, Germany

Abstract: In this contribution the control of a grid-side inverter of a wind energy system (WES) is addressed. Unlike the well-known VOC control strategy, the proposed controller is based on a system model that does not use Park's transformation, i.e. the model is not formulated in d/q -coordinates. Therefore, the system model contains non-linearities, but the validity of the model does not rely on an accurate phase angle detection for the transformation and not on the assumption of a balanced three-phase system. The non-linearities are investigated with the stability theory of Lyapunov and the remaining linear parts can be addressed with methods from linear control theory. The presented control strategy is developed in a simulation environment and numerical simulations were performed. Results are presented that show the effectiveness of the method.

Keywords: grid-side inverter, non-linear, Lyapunov method, transformation, LCL filter

1. INTRODUCTION

Electrical energy is nowadays generated more and more from renewable sources. With this development decentralized power generation, e.g. from wind and solar power, will replace large conventional power plants over time. Naturally, renewable power generation experiences great interest in the industry. Especially wind power is an important energy source in Europe and the most frequent one in Germany (see BMWi (2018)).

Conventional power plants have very good characteristics for stabilizing the energy grid (e.g. the frequency-response reserve) and withstanding grid faults (e.g. by their ability to provide high fault currents). These properties are achieved by large synchronous generators that are directly connected to the energy grid. Concerning renewable power plants, the generators are smaller and not directly connected to the grid. Instead, power electronic inverters are used to establish the grid connection. Thus, renewable power plants like wind energy systems (WES) do not inherently have the good desirable properties like conventional power plants. For this reason, the control algorithms for the inverters of WES must fulfil certain specifications, so that these characteristics can be (in parts) subsequently emulated. These specifications and further regulations are summarized in *TransmissionCodes* (e.g. Berndt et al. (2007)) and are regularly revised. Hence, the control algorithms for the inverters need to be constantly improved.

Voltage Oriented Control (VOC) is a well-known control strategy for grid-side inverters of WES (see e.g. Kazmierkowski et al. (2002), Sanjuan (2010)). VOC uses the d/q -coordinate frame, i.e. Park's transformation is applied to the system model. Because of this, a linear system model is available and methods from linear control theory can be applied to design the current controllers of the inner cascade. The controllers of the outer cascade are also based on a linear model by assuming that only the d -current causes an active power flow at the DC-link capacitor. Typically, all controllers are of PI type and can be parameterized e.g. by following the internal model control (IMC) approach.

Park's transformation is strictly speaking only valid for balanced three-phase systems. And the transformation requires an appropriate phase angle, which can be detected from the measured voltage by a phase-locked loop (PLL). However, the measured voltage is not equal to the stiff grid voltage due to the grid impedance. In cases of high grid impedance the PLL cannot synchronize to the grid properly and the VOC strategy fails. Specifically, the linear models are no longer valid, so the system will behave in unexpected ways and instability of the control loop is likely. Additionally, by using d/q coordinates, the electrical signals (voltages, currents and also the apparent power) are expressed as vectors in the complex plane. This is a useful method, but it is only valid for a constant fundamental frequency. Therefore, it cannot describe transient behaviour accurately, since the PLL needs time to adjust to new operating points.

In this paper a different control strategy is presented. The objective is to relax some of the mentioned assumptions and conduct a more detailed control engineering analysis. The controller is based on a system model that intentionally does not use Park's transformation, so the model

[★] This paper was made within the framework of the research project "Netz-Stabil" and financed by the European Social Fund (ESF/14-BM-A55-0018/16). This paper is part of the qualification programme "Promotion of Young Scientists in Excellent Research Associations - Excellence Research Programme of the State of Mecklenburg-Western Pomerania".

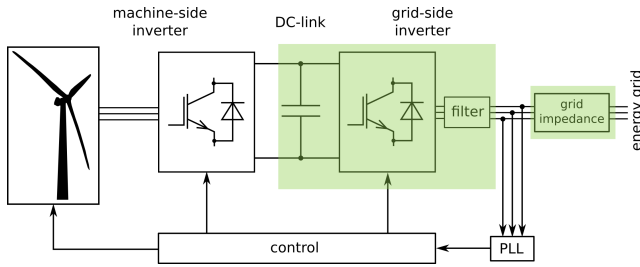


Fig. 1. WES with full scale back-to-back converter (type 4 WES). The important grid-side parts are framed.

contains non-linearities and couplings. With this decision, the control design is more complicated, because methods from linear control theory do no longer apply. But the validity of the model does not depend on an accurate phase angle detection to perform Park's transformation. A PLL is still used in the proposed control strategy to track a phase angle that rotates with the grid frequency. The non-linearities of the model arise from couplings and from multiplications of voltages and currents to calculate the electrical power. These non-linearities are addressed in the time domain. To investigate the stability, Lyapunov's theory is applied. Then, superordinated controllers are proposed to close the control loop, which can be designed with linear methods.

The paper is organized as follows: The next section describes a WES, gives the system model equations and introduces the feed-in control of a WES. Here, the inverter and the grid are modelled as Thévenin-equivalent and an LCL output filter of the inverter is considered. In section 3 the proposed control strategy is developed. Simulation results are given in section 4. The paper closes with a summary and opportunities for future research.

2. SYSTEM DESCRIPTION

In this section the structure of a WES is presented, dynamic models of the relevant parts are derived and the basic feed-in control strategy is described.

The paper considers a type 4 WES, i.e. a WES, that is connected to the energy grid by a full-scale back-to-back inverter (Iov et al. (2008) calls this a *type D* WES). The back-to-back configuration consists of a machine-side and a grid-side inverter and a DC-link circuit in between. The grid-side inverter is additionally equipped with an output filter to suppress high-order harmonics that are caused by the switching behaviour of the inverter. Typically, measurements of the electrical voltages and currents are taken behind the output filter (Teodorescu et al. (2011)). This means, that the ideal grid voltage is not directly measured, but only a voltage, that is altered by the voltage drop across the grid impedance. Nevertheless, the voltage measurement is crucial, because it is used as input to the PLL and has therefore a strong impact on the control system. Fig. 1 shows a functional representation of a the mentioned elements of a type 4 WES and the connection to the energy grid.

The main objective of a WES is to feed electrical energy into the grid. Obviously, the rotor of the WES capture energy from the wind and a generator converts the mechanical energy into electrical energy. More precisely, a

three-phase AC voltage is produced by the generator. The machine-side inverter rectifies the three AC voltages and feeds the energy into the DC-link capacitor, which operates as short-term energy storage. Then, the grid-side inverter generates three-phase AC voltages, but at this point with appropriate amplitude, frequency and phase with respect to the grid voltage. The conversion from AC to DC and vice versa is done by fast-switching power electronics, usually IGBTs (Insulated-Gate Bipolar Transistors).

2.1 System Modelling

The dynamic models of the grid-side parts are now specified. Since the model will be used to design a control strategy, it will not focus on power electronic properties, but on control engineering aspects. Therefore the grid-side inverter is seen as an ideal voltage source, that can generate a sinusoidal voltage with adjustable amplitude and phase angle of the following form (for phase A):

$$U_{Inv,A}(t) = \hat{U}_{Inv}(t) \cos(\varphi_{Inv}(t)). \quad (1)$$

The inverter voltages for phases B and C are the same as (1), only with an additional phase angle shift of $-2/3\pi$ and $-4/3\pi$ respectively. The phase angle is further divided:

$$\varphi_{Inv}(t) = \varphi_{PLL}(t) + \Delta\varphi(t). \quad (2)$$

The value φ_{PLL} is the phase angle that is tracked by the PLL and $\dot{\varphi}_{PLL} = \omega_{grid}$ with ω_{grid} as the angular frequency of the grid holds in steady state. The values \hat{U}_{Inv} and $\Delta\varphi$ are considered as the control input values and both are constant in steady state. Note, that (1) is a non-linear equation with respect to \hat{U}_{Inv} and $\Delta\varphi$.

The energy grid is modelled as Thévenin-equivalent, i.e. it is represented by an ideal voltage source U_{grid} and the grid impedance Z_{grid} in series. It is assumed that the grid impedance consists of an inductance L_{grid} and an additional resistive part R_{grid} . This simple grid model is often applied and is considered as quite sufficient in the literature (see Cobreces et al. (2007), Teodorescu et al. (2011)). As output filter of the grid-side inverter an LCL filter is assumed, i.e. a filter that is composed of two inductances and one capacitor. This filter is formed by the inverter impedance Z_{Inv} (consisting of L_{Inv} and R_{Inv}), a parallel capacitor C_{Inv} and the grid impedance. This model is equal for all three phases of the AC system and the electrical equivalent circuit is shown for one phase in Fig. 2. The dynamic state equations for one phase are (the time and phase index is omitted):

$$\dot{x} = Ax + B_1U_{Inv} + B_2U_{grid} \quad (3)$$

with

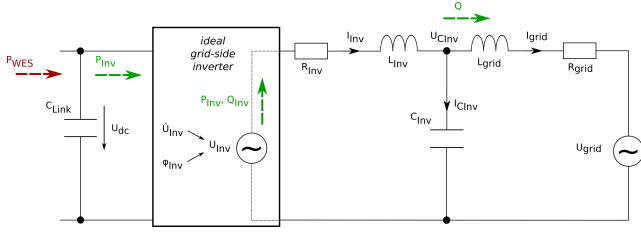


Fig. 2. Equivalent circuit diagram of the grid-side inverter for one phase and the DC-link circuit. Notable power flows are marked in green and red. P_{WES} in red is unknown.

$$x = [I_{Inv} \ I_{grid} \ U_{CInv}]^T \quad (4a)$$

$$A = \begin{bmatrix} -R_{Inv}/L_{Inv} & 0 & -1/L_{Inv} \\ 0 & -R_{grid}/L_{grid} & 1/L_{grid} \\ 1/C_{Inv} & -1/C_{Inv} & 0 \end{bmatrix} \quad (4b)$$

$$B_1 = [1/L_{Inv} \ 0 \ 0]^T \quad (4c)$$

$$B_2 = [0 \ -1/L_{grid} \ 0]^T \quad (4d)$$

and U_{grid} as undisturbed sinusoidal grid voltage: $U_{grid} = \hat{U}_{grid} \cos(\omega_{grid}t + \varphi_{grid,0})$. The state vector x is composed of the inverter current I_{Inv} , the grid current I_{grid} and the filter capacitor voltage U_{CInv} .

The DC-link circuit of the WES is composed of a capacitor. The model of the capacitor (DC-)voltage is (indirectly) given by:

$$\dot{W} = \frac{2}{C_{Link}}(P_{WES} - P_{Inv}). \quad (5)$$

Here, the state transformation $W = U_{dc}^2$ was applied, so that (5) becomes linear in the new state W . P_{WES} denotes the active power from the machine-side inverter that is fed into the DC-link and P_{Inv} the active power of the grid-side inverter (see coloured arrows in Fig. 2). However, if P_{Inv} is expressed with I_{Inv} and U_{Inv} :

$$P_{Inv} = U_{Inv,A} I_{Inv,A} + U_{Inv,B} I_{Inv,B} + U_{Inv,C} I_{Inv,C}, \quad (6)$$

(5) is still non-linear, because it contains multiplications of system states and control inputs.

A common procedure is, that the states I_{Inv} , U_{CInv} are measured (see e.g. Teodorescu et al. (2011)). Additionally, U_{dc} and the reactive power at the filter capacitor Q are also measurement values (see Fig. 2 for the location of Q in the circuit diagram). Furthermore, φ_{PLL} is the phase angle of $U_{CInv,A}$ and is tracked by the PLL. Lastly, W , P_{Inv} , and Q_{Inv} can be calculated from measurements and the control input values.

As PLL a standard SRF-PLL is considered, which will not be discussed in this paper (see e.g. Hoffmann et al. (2011) for detailed information on PLLs).

2.2 Control Objectives of the Feed-in Control

The control objectives are to feed the correct amount of active and reactive power to the energy grid. These objectives have to be met by choosing correct values of

the control input values \hat{U}_{Inv} and $\Delta\varphi$ and applying them to the system.

The active power condition is usually indirectly covered: The objective is to feed the same amount of active power towards the grid that is also generated by the generator of the WES, rectified and fed into the DC-link. Therefore, the control objective could be formulated as: $P_{Inv} = P_{WES}$. Since P_{WES} is unknown, a different control variable is used. From (5) it is clear, that the power balance $P_{Inv} = P_{WES}$ is met, when the DC-link voltage is constant. Hence, the active power condition is indirectly fulfilled, by ensuring $W = U_{dc}^2 = const$ and a typically desired value is $U_{dc,des} = 1100 \text{ V}$.

The desired amount of reactive power Q_{des} is either given by the grid operator or determined by regulations in the TransmissionCodes. $Q = Q_{des}$ has to be fulfilled at the output filter capacitor (see Fig. 2 for the location of Q).

In addition to these control objectives, further constraints have to be met. One important criterion is to limit the amplitude of the currents, because, in contrast to synchronous machines, inverters cannot endure currents over approximately 1,5 times the nominal value. To comply with this, the control inputs should remain within certain intervals. Insight to these interval limits can be gained by assuming a decoupled system: Following Fazli et al. (2018), the control input \hat{U}_{Inv} controls mainly Q and $\hat{U}_{Inv} = \hat{U}_{grid}$ corresponds with a reactive power of zero. Q_{des} is usually small compared to P_{Inv} and can be positive or negative, so \hat{U}_{Inv} should be around \hat{U}_{grid} with an upper limit of U_{dc} (the exact upper limit depends on the modulation type of the inverter) and a meaningful lower limit (e.g. 80% of \hat{U}_{grid}). On the other hand, the control input $\Delta\varphi$ controls mainly P_{Inv} and only positive P_{Inv} are allowed, because there should be no power flow from the grid back to the WES in the nominal case. Therefore the lower limit is $\Delta\varphi = 0$. An upper limit can be set by $\pi/2$ (see e.g. Saadat (1999)).

The control objectives of the feed-in control can be summarized in the following way: Choose appropriate values for \hat{U}_{Inv} and $\Delta\varphi$ so that the objectives (7) are met and the conditions (8) hold:

$$U_{dc} = 1100 \text{ V} \quad (7a)$$

$$Q = Q_{des} \quad (7b)$$

$$\hat{U}_{Inv} \in [0, 8 \hat{U}_{grid}; U_{dc}] \quad (8a)$$

$$\Delta\varphi \in [0; \pi/2]. \quad (8b)$$

In the next section a strategy is presented to accomplish these control objectives.

3. CONTROL STRATEGY

In contrast to VOC, the proposed control scheme does not rely on Park's transformation and is directly applied to the model equation that results from inserting (6) into (5). Since this equation is non-linear, standard methods from linear control engineering are not suitable and other

methods have to be applied. Here, a transformation is derived from (5) and the Lyapunov method from non-linear control theory is applied to investigate the stability. The non-linear control law is then supplemented with two superordinated controllers to achieve the objectives (7). It will be seen, that these additional controllers can be designed with linear design methods.

3.1 Non-linear Control Law

From (5) it is clear, that a constant W (and thus also a constant U_{dc}) is achieved when the active input power and the active output power of the DC-link are balanced. It is initially assumed, that this balance is fulfilled by

$$P_{Inv} = P_{Inv,des}. \quad (9)$$

Applying (1), (2), (6), and trigonometric formulas, (9) can be rewritten:

$$P_{Inv,des} = \hat{U}_{Inv} (k_1 \cos \Delta\varphi + k_2 \sin \Delta\varphi). \quad (10)$$

The terms k_1 and k_2 are listed in appendix A. Note, that k_1 and k_2 can be calculated, since they are composed of known signals only.

A similar consideration can be done for the reactive power as well. Under the assumption of a symmetric three-phase system, the reactive power of the inverter is given by:

$$Q_{Inv} = \frac{1}{\sqrt{3}} [(U_{Inv,B} - U_{Inv,C})I_{Inv,A} + (U_{Inv,C} - U_{Inv,A})I_{Inv,B} + (U_{Inv,A} - U_{Inv,B})I_{Inv,C}]. \quad (11)$$

Assume, that the desired value Q_{des} at the filter capacitor is achieved by $Q_{Inv} = Q_{Inv,des}$. By using (1), (2), (11), and trigonometric formulas this can be reformulated:

$$Q_{Inv,des} = \frac{\hat{U}_{Inv}}{\sqrt{3}} (k_3 \cos \Delta\varphi + k_4 \sin \Delta\varphi). \quad (12)$$

Again, k_3 and k_4 are specified in appendix A and both can be calculated from measured signals.

Equations (10) and (12) can be solved for $\Delta\varphi$ and \hat{U}_{Inv} . The analytical solutions are:

$$\Delta\varphi = \arctan \left(\frac{\sqrt{3}k_1 Q_{Inv,des} - k_3 P_{Inv,des}}{k_4 P_{Inv,des} - \sqrt{3}k_2 Q_{Inv,des}} \right) \quad (13a)$$

$$\hat{U}_{Inv} = \frac{P_{Inv,des}}{(k_1 \cos \Delta\varphi + k_2 \sin \Delta\varphi)}. \quad (13b)$$

One observation is, that the solution (13) does not always provide control inputs that fit the control input constraints (8). If this case occurs, a different solution has to be found. A possible procedure is sketched here: The objective is to find \hat{U}_{Inv} and $\Delta\varphi$, that exactly fulfil (10) (i.d. the active power condition is prioritized) and that fulfil (12) with the least discrepancy. To achieve this, (10) and (12)

can be rearranged and the following cost function can be established:

$$J = \left| \frac{P_{Inv,des}}{(k_1 \cos \Delta\varphi + k_2 \sin \Delta\varphi)} - \frac{\sqrt{3}Q_{Inv,des}}{(k_3 \cos \Delta\varphi + k_4 \sin \Delta\varphi)} \right|. \quad (14)$$

The $\Delta\varphi$ is sought, that minimizes J under the constraints (8). An analytical solution is difficult to obtain, but numerical methods can yield a minimum, e.g. a line search method. By using different initial values, the reliability of the solution can be increased. Then, \hat{U}_{Inv} is calculated using (13b).

In summary, this non-linear law transforms the demands of active and reactive power $P_{Inv,des}$ and $Q_{Inv,des}$ to appropriate control input values \hat{U}_{Inv} and $\Delta\varphi$.

3.2 Considerations on Stability

Since the derived control law from section 3.1 is non-linear, the stability cannot be determined by linear methods. Instead, the Lyapunov stability theory (see e.g. Aström and Wittenmark (2008)) is applied to the DC-link voltage. Since the Lyapunov method assumes zero as the control objective, a state transformation is applied:

$$z = \sqrt{W} - 1100. \quad (15)$$

As Lyapunov function $V(z)$ the energy of the DC-link capacitor is chosen:

$$V(z) = \frac{1}{2} C_{Link} z^2. \quad (16)$$

The first time derivative of (16) is $\dot{V}(z) = C_{Link} z \dot{z}$. With (5) and (15) this becomes:

$$\dot{V}(z) = \frac{z}{z + 1100} (P_{WES} - P_{Inv}). \quad (17)$$

The condition for *asymptotic* stability is $\dot{V}(z) < 0$. It is clear from (17) that by exactly fulfilling the power balance, only $\dot{V}(z) = 0$ can be achieved, which is only sufficient in steady-state, i.e. when $U_{dc} = 1100 V$ is already reached. So, when steady state is not reached yet, the control inputs are slightly modified. By inserting (1) into (6) the following can be concluded:

$$P_{Inv} = \hat{U}_{Inv} [I_{Inv,A} \cos(\varphi_{Inv}) + I_{Inv,B} \cos(\varphi_{Inv} - 2/3\pi) + I_{Inv,C} \cos(\varphi_{Inv} - 4/3\pi)]. \quad (18)$$

Hence, P_{Inv} can be marginally increased or decreased by adding or subtracting a small value (e.g. 1 V) to \hat{U}_{Inv} . Depending on the factor $\frac{z}{z+1100}$ in (17) this can be done to ensure $\dot{V}(z) < 0$ and thus a stable control law in the sense of Lyapunov.

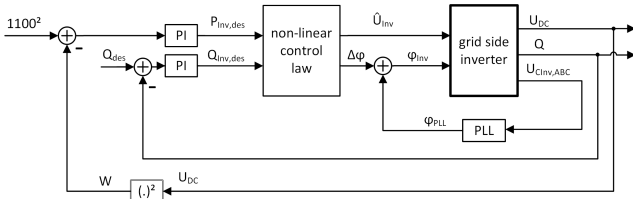


Fig. 3. Block diagram of the control scheme.

3.3 Superordinated Controllers

In section 3.1 it was assumed that the values $P_{Inv,des}$ and $Q_{Inv,des}$ are known. This situation does not generally apply. But additional superordinated controllers can be used to address this issue. These controllers take the control deviations $1100^2 - W$ and $Q_{des} - Q$ as inputs and provide $P_{Inv,des}$ and $Q_{Inv,des}$ to the non-linear control law. For this task linear PI controllers are applicable, because (5) can be directly used as system model. The PI controllers are realised in the form $u = K_p e + K_i \int e dt$. The complete control scheme is presented as block diagram in Fig. 3.

The parameters of the U_{dc}^2 -controller were designed by following an internal model control (IMC) approach, that was proposed in Ottersten (2003) for inverter control. The Q -controller was designed in the same way, but was slowed down by a factor of 5.

4. SIMULATION RESULTS

To test the proposed control strategy, numerical simulations were carried out. The dynamic model equations (3) and (5) as well as the static power calculation (6) and (11) were set up in Matlab/Simulink and the non-linear control scheme from section 3 was implemented. The simulation parameters are given in table 1.

Table 1. Simulation parameters

parameter	value	parameter	value
\hat{U}_{grid}	$690\sqrt{2/3} V$	ω_{grid}	$2\pi 50 rad/s$
R_{grid}	$3,2 m\Omega$	$K_{P,PLL}$	0,22
L_{grid}	$51,43 \mu H$	$K_{I,PLL}$	5,26
R_{Inv}	$3,1 m\Omega$	$K_{P,U_{dc}}$	-1,10
L_{Inv}	$49,54 \mu H$	$K_{I,U_{dc}}$	-241,39
C_{Inv}	$5 mF$	$K_{P,Q}$	0,22
C_{Link}	$10 mF$	$K_{I,Q}$	9,66

Table 2. Changes of impedances from nominal value to form an unbalanced three-phase system

impedance	phase A	phase B	phase C
R_{grid}	-10%	-20%	+20%
L_{grid}	10%	20%	-20%
R_{Inv}	-20%	0%	+30%
L_{Inv}	+20%	0%	-20%
C_{Inv}	0%	-30%	+20%

For comparison, a standard VOC strategy was also implemented and tested in the same environment. The outer cascade VOC controllers were designed in the same manner as the superordinated controllers of the non-linear strategy: the IMC approach was applied to the U_{dc}^2 -controller with the same specified rise time and the Q

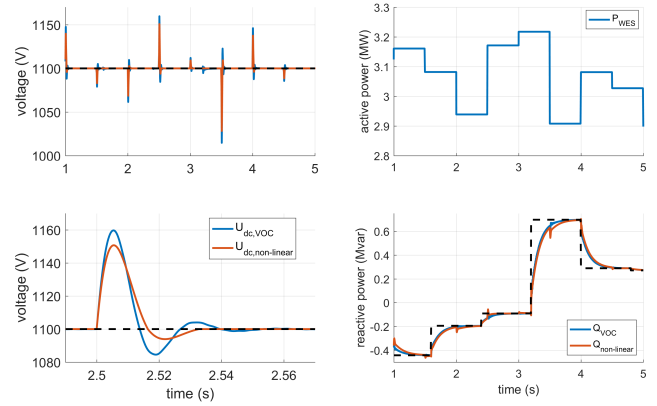


Fig. 4. Left: courses of U_{dc} at different zoom levels with the desired value in black. Top right: step-like changes of P_{WES} around the nominal value of 3 MW. Bottom right: desired value of Q in black and actual courses of Q .

controller was slowed down by a factor of 5. The inner cascade current controllers were parameterized with a 3 times faster rise time.

The simulations were performed with a desired value for the DC-link voltage of 1100 V, but the DC-link circuit was excited in the experiments with step-like changes of P_{WES} around the nominal value of 3 MW. This excitation is not realistic with respect to the application, but step-like changes are typical test cases in control engineering and can be considered as a worst case scenario. The P_{WES} curve can be seen on the top right of Fig. 4. In a similar manner, the desired value of the reactive power also changes during the simulations.

The results of the first experiment can be seen in Fig. 4. The left side of the figure shows the DC-link voltage at the top and a different zoom level of the same curve at the bottom. On the bottom right the values for the desired reactive power and the actual reactive power are depicted. It can be seen that after each excitation the set point of the DC-link voltage is reached again and that the non-linear controller achieves this faster and with smaller overshoots. Considering the reactive power, the VOC controller shows better performance: the desired value is reached a bit faster and the cross-influence of a P_{WES} change is noticeably smaller, which can be seen by the dips of $Q_{non-linear}$ (e.g. at $t = 3,5 s$) in Fig. 4. This effect is due to the prioritization of the active power condition in the non-linear controller.

For more realistic circumstances, measurement noise is added to U_{dc} , I_{Inv} and U_{CInv} in a second experiment. Additionally, the impedances of the model are changed at $t = 2,5 s$ according to table 2, so that an unbalanced three-phase system is present. The results are shown in Fig. 5. Again, both controllers achieve the desired values. But the plots prove, that the non-linear controller shows less unsteady behaviour in the presence of noise and a considerably improved performance without oscillations of U_{dc} in the case of unbalanced impedances. This advantage originates from the fact that the non-linear controller does not use Park's transformation, which assumes a balanced system.

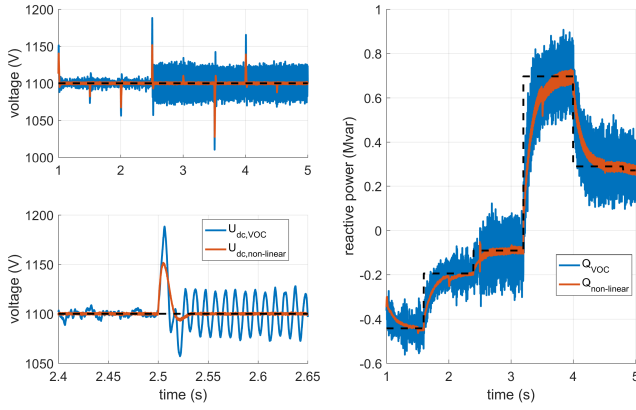


Fig. 5. Experiment with measurement noise and unbalanced impedances from 2.5 s. Left: courses of U_{dc} at different zoom levels with the desired value in black. Right: desired value of Q in black and actual courses of Q .

5. SUMMARY

The control of a grid-side inverter was addressed in this paper. Dynamic models of the inverter, the DC-link circuit and the grid impedance were presented in abc -coordinates, i.e. without applying Park's transformation. Therefore, certain non-linearities remained in the system model intentionally. A non-linear control scheme was suggested to control the active and reactive power of the inverter, whereby the active power is controlled indirectly through the DC-link voltage. The controller scheme is composed of a non-linear control law and two superordinated linear controllers, each for one of the control values. Lyapunov's theory was applied to investigate the stability properties. Numerical simulations were conducted to show the functionality of the proposed control scheme.

Since the controller considers non-linearities and does not rely on Park's transformation it can cover a broader range of operating points and additional effects. The simulations show for example that unbalanced impedances are handled with improved performance when compared to the standard VOC strategy. The presented approach can be seen as a partial result for non-linear analysis and control design for grid-side inverters. Specific aspects of the suggested controller must be further investigated, e.g. the behaviour during typical error scenarios, like phase shifts. Currently the controller also lacks the ability to countermeasure possible over-currents (besides the constraints on the control input values). These features will be investigated in future research.

REFERENCES

- Aström, K. and Wittenmark, B. (2008). *Adaptive Control*. Dover Publications, Mineola, N.Y.
- Berndt, H., Hermann, M., Kreye, H., Reinisch, R., Scherer, U., and Vanzetta, J. (2007). *TransmissionCode 2007*. Verband der Netzbetreiber, Berlin.
- BMWi (2018). *Sechster Monitoring-Bericht zur Energiewende (Sixth Monitoring Report on the Transition to Renewable Energy Generation)*. Bundesministerium für Wirtschaft und Energie, Berlin.

- Cobreces, S., Huerta, F., Pizarro, D., Rodriguez, F., and Bueno, E. (2007). Three-phase power system parametric identification based on complex-space recursive least squares. In *2007 IEEE International Symposium on Intelligent Signal Processing*.
- Fazli, N., Gierschner, S., Gierschner, M., Cai, L., and Eckel, H.G. (2018). Rotating-Voltage-Vector Control for Wind Energy Plants providing Possibility for Ancillary Services. In *2018 20th European Conference on Power Electronics and Applications*.
- Hoffmann, N., Lohde, R., Fischer, M., Fuchs, F.W., Asiminoaei, L., and Thogersen, P.B. (2011). A Review on Fundamental Grid-Voltage Detection Methods under Highly Distorted Conditions in Distributed Power-Generation Networks. In *2011 IEEE Energy Conversion Congress and Exposition*.
- Iov, F., Ciobotaru, M., and Blaabjerg, F. (2008). Power Electronics Control of Wind Energy in Distributed Power Systems. In *2008 11th International Conference on Optimization of Electrical and Electronic Equipment*.
- Kazmierkowski, M.P., Krishnan, R., and Blaabjerg, F. (eds.) (2002). *Control in Power Electronics: Selected Problems*. Academic Press, New York.
- Ottersten, R. (2003). *On Control of Back-to-Back Converters and Sensorless Induction Machine Drives*. Ph.D. thesis, Chalmers University of Technology, Göteborg.
- Rocabert, J., Luna, A., Blaabjerg, F., and Rodriguez, P. (2012). Control of Power Converters in AC Microgrids. *IEEE Transactions on Power Electronics*, 27(11), 4734–4749.
- Saadat, H. (1999). *Power System Analysis*. WCB/McGraw-Hill, Boston.
- Sanjuan, S. (2010). *Voltage Oriented Control of Three-Phase Boost PWM Converters*. Master's thesis, Chalmers University of Technology, Göteborg.
- Teodorescu, R., Liserre, M., and Rodriguez, P. (2011). *Grid Converters for Photovoltaic and Wind Power Systems*. IEEE ; Wiley, Chichester, West Sussex ; Hoboken, N.J.

Appendix A. EXPRESSIONS FOR ABBREVIATED TERMS

$$\begin{aligned}
 k_1 &= I_{Inv,A} \cos \varphi_{PLL} \\
 &\quad - 1/2 I_{Inv,B} \cos \varphi_{PLL} + \sqrt{3}/2 I_{Inv,B} \sin \varphi_{PLL} \\
 &\quad - 1/2 I_{Inv,C} \cos \varphi_{PLL} - \sqrt{3}/2 I_{Inv,C} \sin \varphi_{PLL} \\
 k_2 &= - I_{Inv,A} \sin \varphi_{PLL} \\
 &\quad + 1/2 I_{Inv,B} \sin \varphi_{PLL} + \sqrt{3}/2 I_{Inv,B} \cos \varphi_{PLL} \\
 &\quad + 1/2 I_{Inv,C} \sin \varphi_{PLL} - \sqrt{3}/2 I_{Inv,C} \cos \varphi_{PLL} \\
 k_3 &= \sqrt{3} I_{Inv,A} \sin \varphi_{PLL} \\
 &\quad - 3/2 I_{Inv,B} \cos \varphi_{PLL} - \sqrt{3}/2 I_{Inv,B} \sin \varphi_{PLL} \\
 &\quad + 3/2 I_{Inv,C} \cos \varphi_{PLL} - \sqrt{3}/2 I_{Inv,C} \sin \varphi_{PLL} \\
 k_4 &= \sqrt{3} I_{Inv,A} \cos \varphi_{PLL} \\
 &\quad + 3/2 I_{Inv,B} \sin \varphi_{PLL} - \sqrt{3}/2 I_{Inv,B} \cos \varphi_{PLL} \\
 &\quad - 3/2 I_{Inv,C} \sin \varphi_{PLL} - \sqrt{3}/2 I_{Inv,C} \cos \varphi_{PLL}
 \end{aligned}$$